Compression Behavior of Zr-doped Nanoanatase

Eva Holbig[a], Leonid Dubrovinsky[a], Gerd Steinle-Neumann[a], Vitali Prakapenka[b], and Varghese Swamy[c]

[a] Bayerisches Geoinstitut, University of Bayreuth, D-95440 Bayreuth, Germany
[b] GeoSoilEnviroCARS, University of Chicago, Chicago, 60637, USA
[c] Department of Materials Engineering, Monash University, P. O. Box 69M, Victoria 3800, Australia

Reprint requests to Eva Holbig. Fax: +49 921 553769. E-mail: Eva.Holbig@Uni-Bayreuth.de

Z. Naturforsch. **61b,** 1577 – 1585 (2006); received September 22, 2006

The compression behavior of Zr-doped nano anatase $Ti_{0.90}Zr_{0.10}O_2$ synthesized by the sol-gel method was studied using a diamond anvil cell (DAC) up to $\sim$ 13 GPa. The compressibility parallel to the *a* axis decreases strongly at $\sim$ 4 GPa and other structural parameters also change with pressure. The parameters of the third order Birch-Murnaghan equation of state were fitted to: V_0 = 139.6(0) Å^3, K_0 = 213(9) GPa and K' = 17.9(2). *Ab initio* electronic structure simulations indicate that the Zr atoms cluster in the crystal. The effects of chemical substitution as well as of microstructure, especially the crystallite size, on the mechanical properties are discussed.

Key words: High-pressure, Nanocrystals, Titania, Zirconia, Anatase, Dopant

Introduction

Titania TiO_2, zirconia ZrO_2, as well as zirconium-titanium oxides and zirconium titanate based materials are technologically and industrially important functional ceramics used, *e. g.*, for pigments [1, 2], composite materials [3, 4] or catalysts and catalyst supports [5]. At high pressures and temperatures, TiO_2 and ZrO_2 exist in a number of polymorphs. At pressures $<$ 5 GPa the stable form of TiO_2 is rutile (tetragonal, space group $P4_2/mnm$, coordination number CN = 6), but also anatase (tetragonal, $I4_1/amd$, CN = 6) and brookite (tetragonal, *Pcab*, CN = 6) exist as metastable forms as well as a number of other modifications [6]. High-pressure polymorphs are the orthorhombic forms TiO_2-II (columbite structure, space group *Pbcn*, CN = 6) at pressures of 5 to 8 GPa [7 – 9], MI (baddeleyite structure, $P2_1/c$, CN = 7) to 20 GPa [10, 11] and OI (*Pbca*, CN = 7) to 50 GPa [12], and at higher pressures OII (cottunite structure, *Pnma*, CN = 9) [13, 14] along with a cubic phase with the space group $Fm\bar{3}m$ or $Pa\bar{3}$ and CN = 9 [15] (see also references in Table 1).

The ZrO_2 polymorphs stable at ambient pressures are monoclinic baddeleyite, also referred to as MI, with the space group $P2_1/c$ and CN = 7 for Zr. At temperatures above 1200 °C a tetragonal phase with space group $P4_2/nmc$ and CN = 7 occurs. Above 2372 °C a cubic fluorite-type structure with space group $Fm\bar{3}m$ and CN = 8 is stable, and at 2680 °C the melting point is reached [16]. Baddeleyite is stable up to 10 GPa, the polymorphs at higher pressures are orthorhombic: OI (space group *Pbca*, CN = 7) at pressures $<$ 25 GPa and OII (*Pnam*, CN = 9) at pressures $<$ 42 GPa [17]. The values given by Ohtaka *et al*. [18] for the stabilities of the high-pressure polymorphs differ strongly from the ones given above: baddeleyite $<$ 3 – 4 GPa, OI $<$ 12.5 GPa and OII $<$ 24 GPa. Both groups of authors suggest a cotunnite structure for OII and describe an orthorhombic phase, OIV, which is stable at higher temperatures than OII and at higher pressures than the tetragonal phase with the space group being most likely $Pbc2_1$.

The compressibility of high-pressure polymorphs of TiO_2 is systematically smaller than for ZrO_2, indicated by higher bulk moduli K_0 for TiO_2. For the monoclinic MI phase, K_0 was measured as 290 – 303 GPa for TiO_2 and as 187 – 212 GPa for ZrO_2. The values of K_0 for the orthorhombic phases are 318 GPa (TiO_2) and 243 GPa (ZrO_2) for OI, and 431 GPa (TiO_2) and 265 – 444 GPa (ZrO_2) for OII, respectively (details, nomenclature, and references are given in Table 1). This pattern can be understood by a comparison of the electronic structures of Zr and Ti: Having one more electron shell, Zr has larger ionic and covalent radii than Ti and therefore a higher compressibility. However, the

Table 1. Volumes and bulk moduli of TiO_2 and ZrO_2 polymorphs.

*K*o = isothermal bulk modulus; V = elementary cell volume; Z = number of TiO_2 or ZrO_2 per elementary cell; DAC = diamond anvil cell; XRD = *in situ* X-ray diffraction; MA = multianvil; MD = molecular dynamics; Brill. scat. = Brillouin scattering; f = fixed value.

Phase	V_0 (Å^3)	V_0/Z (Å^3)	K_0 (GPa)	K'_0	P (GPa)	T (K)	Technique	Ref.
TiO_2								
rutile	62.5	31.2	230(20)	6.6(7)	0 – 20	300	DAC + XRD	[47]
rutile	62.5	31.2	210(10)	6.6(7)	0 – 8	300	MA + XRD	[8]
anatase	136.8	34.2	178(1)	4 *f*	0 – 8	300	DAC + XRD	[20]
anatase	136.3	34.1	190(10)	5.3(10)	0 – 14	300	DAC + XRD	[23]
anatase	143.8	36.0	189.5	3.4	0 – 50	–	*ab initio*	[23]
anatase (single cryst.)	136.3	34.1	179(2)	4.5(10)	0 – 5	300	DAC + XRD	[23]
anatase (30 – 40 nm)	136.2	34.0	243(3)	4 *f*	0 – 35	300	DAC + XRD	[21]
anatase (6 nm)	–	–	237(3)	4 *f*	6 – 18	300	DAC + XRD	[46]
anatase (6 nm)	–	–	260	4 *f*	15	–	MD	[46]
anatase (6 nm)	–	–	240	4 *f*	20	–	MD	[46]
Zr-anatase	139.6(0)	34.9	213(9)	17.9(2)	0 – 13	300	DAC + XRD	this study
Zr-anatase	139.4(1)	34.9	278.7(7.0)	4 *f*	0 – 13	300	DAC + XRD	this study
Zr-anatase	139.5(0)	34.9	249(6)	4 *f*	0 – 5	300	DAC + XRD	this study
Zr-anatase	139.1(1)	34.8	301(1)	4 *f*	4 – 13	300	DAC + XRD	this study
anatase	141.1	35.3	153.0	4	−8 – 34	0	*ab initio*	this study
Zr-anatase	145.4	36.4	161.0	4	−10 – 46	0	*ab initio*	this study
brookite	257.8	32.2	255(10)	4 *f*	0 – 8	300	DAC + XRD	[48]
MI	112.2	28.1	290(20)	4 *f*	10 – 60	300	DAC + XRD	[47]
MI	112.2	28.1	290(20)	4 *f*	0 – 20	300	MA + XRD	[8]
MI	105.1	26.3	304(6)	3.9(2)	30 – 80	300	DAC + XRD	[20]
α-PbO2	122.4	30.6	260(30)	–	0 – 10	300	DAC + XRD	[47]
α-PbO2	122.4	30.6	258(8)	4.05(25)	0 – 8	300	MA + XRD	[8]
OI	109.1	27.3	318(3)	4 *f*	19 – 36	300	DAC + XRD	[12]
OII	105.1	26.3	431(10)	1.35(10)	15 – 42	300	DAC + XRD	[20]
cubic	115.5	28.9	202(5)	1.3(1)	10 – 55	300	DAC + XRD	[15]
ZrO_2								
MI	140.6	35.2	212(24)	8(4)	0 – 70	300	DAC + XRD	[49]
MI	–	–	187	–	0	–	Brill. scat.	[50]
MI	–	–	152	4.00	–	–	*ab initio*	[51]
MI	–	–	157	2.38	–	–	*ab initio*	[52]
tetragonal (nanocryst.)	139.4	34.9	172(6)	8.5(5)	0 – 10	300	DAC + XRD	[53]
tetragonal	–	–	205(10)	4 *f*	0 – 12.5	1000	MA + XRD	[18]
tetragonal	–	–	200	6.25	–	–	*ab initio*	[52]
OI	134.0	33.5	243(10)	7(2)	10 – 25	300	DAC + XRD	[49]
OI	–	–	273	3..51	–	–	*ab initio*	[51]
OI	–	–	272	4.63	–	–	*ab initio*	[52]
OII	123.2	30.8	444(15)	1 *f*	0 – 70	300	DAC + XRD	[49]
OII	120.1	30.0	265(10)	4 *f*	0 – 24	300	MA + XRD	[18]
OII	120.1	30.0	296(5)	1 *f*	0 – 24	300	MA + XRD	[18]
OII	120.9	30.2	306(10)	3.66 *f*	0 – 50	300	DAC + XRD	[55]
OII	120.9	30.2	322(8)	2.3(4)	0 – 50	300	DAC + XRD	[55]
OII	120.0	30.0	278(11)	3.70(22)	0 – 100	300	DAC + XRD	[54]
OII	120.0	30.0	267(3)	4 *f*	0 – 100	300	DAC + XRD	[54]
OII	–	–	314	3.66	–	–	*ab initio*	[51]
OII	–	–	305	4.68	–	–	*ab initio*	[52]

compression behavior of Ti and Zr oxides is not only controlled by the compressibility of the metal atoms, but also by the distortion of their coordination polyhedra and of the oxygen atoms. The octahedra of most polymorphs are distorted and baddeleyite, the ZrO_2 polymorph stable at ambient conditions, or TiO_2-II, a high-pressure polymorph of TiO_2, consist of ZrO_7 and TiO_7 polyhedra. The valence electrons in the *d* states play an important role in the distortion of the polyhedra [19].

Apart from its (ideal) crystal structure, the compression behavior of a material is also controlled by the

microstructure as well as by stress and strain in the crystallites. A decrease in crystallite size leads to a higher bulk modulus for anatase, as shown by Swamy and Dubrovinsky [20, 21]. The authors carried out experiments on the compression behaviour of macrocrystalline anatase [20] up to 8 GPa as well as of nanocrystalline anatase [21] up to 35 GPa. The pressure-volume data were fitted to a second-order Birch-Murnaghan equation of state (EoS) [22]. They determined the isothermal bulk modulus for macrocrystalline anatase to be 178(1) GPa. The value for the nanocrystalline counterpart is 243(3) GPa, which is about 35% larger. The results suggest that stress hardens the material.

Stress and strain also affect the limit for transformations into high-pressure polymorphs. *E. g.*, a decrease in crystallite size apparently stabilizes anatase up to higher pressures: Anatase single crystals transform into TiO_2-II at 2.5 GPa [11] and 4.5 GPa [23]. The transformation of polycrystalline anatase into TiO_2-II was found at 2.6 GPa [24], 7 GPa [25] and 5 GPa [26]. The transformation of TiO_2-II into the MI structure occurred at 10 GPa [26], 12 – 15 GPa [26], and 13 – 17 GPa [11]. A number of experimental studies [21, 23, 27] showed a transformation of nano- and fine-grained polycrystalline anatase into MI at pressures $\geq$ 13 GPa. This result led to the conclusion that a decrease in crystallite size suppresses the formation of TiO_2-II and leads to a higher pressure limit of the transformation anatase $\rightarrow$ MI.

In this study, we focus on the variation of compressibility of anatase in response to doping with Zr. Information is gained about the differences in the compression behavior of Ti and Zr oxides, about the effect of substitution of atoms on the compressibility and of the microstructure, especially the crystallite size, on the elastic properties.

Experimental and Computational Procedures

Compression experiments

Experiments were carried out in the 4 pin diamond anvil cell (DAC) manufactured at Bayerisches Geoinstitut [28], using a pair of 1/4 karate type IA diamonds with a cullet size of 300 μm. Rhenium foil with 250 μm thickness was pre-indented to 40 – 50 μm and a hole of $\sim$ 120 μm was drilled to form the gasket. As starting material we used nanocrystalline Zr-doped anatase $Ti_{0.90}Zr_{0.10}O_2$, synthesized with the sol-gel process [29] which was homogeneously mixed with LiF (99.99% purity) in a proportion of about

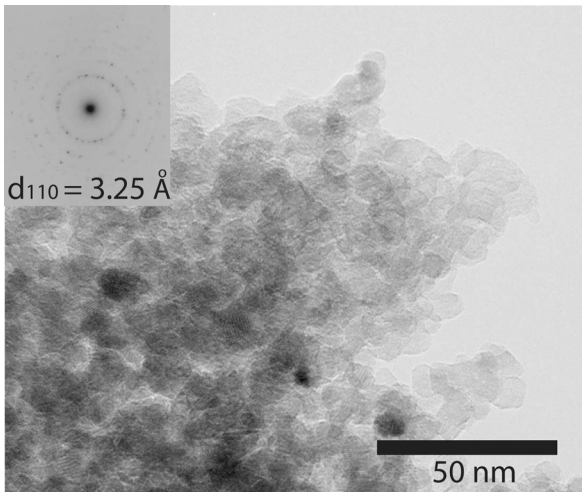

Fig. 1. High-resolution TEM image of the starting material anatase $Zr_{0.1}Ti_{0.9}O_2$, indicating average crystallite sizes of $\sim 15(\pm 5)$ nm.

1 : 1 [w/w]. The crystallite size of the doped anatase was about 15($\pm$5) nm, as indicated by high-resolution transmission electron microscopy (Fig. 1) and confirmed by convolution-based profile fitting of X-ray powder diffraction data. We used LiF both as internal pressure standard [30] and as a relatively soft pressure-transmitting medium. *In situ* angle-dispersive diffraction patterns were collected at the GeoSoilEnviroCARS 13 BMD at the Advanced Photon Source (APS), Argonne, Illinois. We used MAR345 as a detector and an X-ray beam with a wavelength of 0.31 Å and a size of 6×15 μm. The distance sample to detector was 272 mm. The seats of the DAC had an opening of 22° allowing the collection of diffraction data to $\sim$ 1 Å^3. The diffraction images were integrated using the FIT2D program [31], full profile refinements were done using the GSAS program [32, 33]. The standard deviation of the LiF volume at the maximum pressure achieved (13 GPa) is less than 0.01 Å^3, corresponding to an uncertainty in pressure of less then 0.5 GPa.

First principle calculations

We performed *ab initio* density functional electronic structure simulations, using the projector-augmented wave (PAW) method [34] in the generalized gradient approximation (GGA) to the exchange correlation potential [35] and a plane wave basis set as implemented in the Vienna Ab-Initio Simulation Package (VASP) [36, 37]. We calculated ground state energetics (zero temperature) of Ti_8O_{16} as well as $Zr_1Ti_7O_{16}$ supercells

for varying volumes and explored the variation of cell parameters, energies and atomic positions as a function of the volume. As starting point, we used an experimentally determined anatase cell with lattice parameters a = 3.7842, c = 9.5146 Å and V = 136.25 Å^3 [38]. Ti occupies the Wyckoff position *4a* (0, 0, 0), oxygen occupies *8e* (0, 0, 0.21). We used a $2 \times 1 \times 1$ supercell for anatase for the computations as well as a Zr doped version of this cell ($Zr_1Ti_7O_{16}$). Reciprocal space was sampled on a $6 \times 12 \times 4$ Monkhorst-Pack k point grid [39]. Both cells were relaxed for internal and external degrees of freedom. Leaving the volume fixed for volumes ranging from 10.0 – 12.5 for TiO_2 and 10.0 – 13.0 Å^3 per atom for $ZrTi_7O_{16}$. The symmetry was found to be stable in the anatase structure even in the Zr-doped anatase.

In order to gain insight into the Zr-distribution in the TiO_2-ZrO_2 solid solution close to the composition studied experimentally, and to investigate the possible tendency of clustering of zirconium atoms we performed computations on alternative supercells. Computations were conducted on cells with a volume of 11.0 Å^3 per atom and the ratio of Ti : Zr = 7 : 1. In the Ti-Zr supercell mentioned before the a parameter is doubled while b and c remain the same as in anatase, our notation is therefore $2a \times b \times c$. In this cell, next neighboring Zr atoms with a distance of 3.78 Å are found along the b direction. A different supercell with the setup $a \times b \times 2c$ has next neighboring Zr atoms with the same distance in both, a and b directions and therefore shows a tendency of clustering when compared to the $2a \times b \times c$ cell. In another supercell, the Zr atoms are spread equally, opposing the tendency of clustering. The setup is $2a \times 2b \times c$ and the next neighboring Zr atoms have a distance of 5.38 Å. The cell has a doubled size and two Zr atoms are placed in the positions 0, 0, 1/2 and 0, 1/2, 1/8. For all supercells, we calculated the forces and the stress tensors under relaxation of ions and cell shape, using k point meshes of $6 \times 12 \times 4$ for $2a \times b \times c$, $12 \times 12 \times 2$ for $a \times b \times 2c$ and $4 \times 4 \times 4$ for $2a \times 2b \times c$.

Experimental results

The lattice parameters of Zr-doped anatase at zero pressure were refined to a = 3.8110(3), c = 9.6101(12) Å and V = 139.57(2) Å^3. As the larger Zr is incorporated for the smaller Ti into the structure, the values are consistently higher than the ones for pure anatase obtained by Swamy *et al.* [20, 21]. The authors report a = 3.7910(5), c = 9.5146(9) Å and V = 136.74(5) Å^3 for macrocrystalline anatase [20] and a = 3.7830(3), c = 9.513(9) Å and V = 136.15(2) Å^3 for nanocrystalline anatase with crystallite sizes of 30 to 40 nm [21]. The trend is consistent with the data presented by Holbig *et al.* [29] of lattice parameters refinements of different phases in the system TiO_2-ZrO_2.

Table 2. Experimental lattice parameters and oxygen positions.

p(GPa)	a (Å)	c (Å)	V (Å^3)	z(Ox)
0	3.8110(3)	9.610(1)	139.57(2)	0.0827(3)
1.2(1)	3.8062(4)	9.583(3)	138.83(5)	0.088(1)
1.7(2)	3.8014(7)	9.588(6)	138.56(9)	0.077(2)
3.0(2)	3.7957(9)	9.568(7)	137.8(1)	0.073(2)
4.1(3)	3.791(1)	9.555(9)	137.3(1)	0.068(3)
5.2(3)	3.788(1)	9.54(1)	136.8(2)	0.069(3)
7.7(4)	3.780(1)	9.49(1)	135.6(2)	0.071(3)
10.3(4)	3.776(2)	9.44(1)	134.6(2)	0.073(3)
13.0(5)	3.775(2)	9.38(1)	133.7(2)	0.075(4)

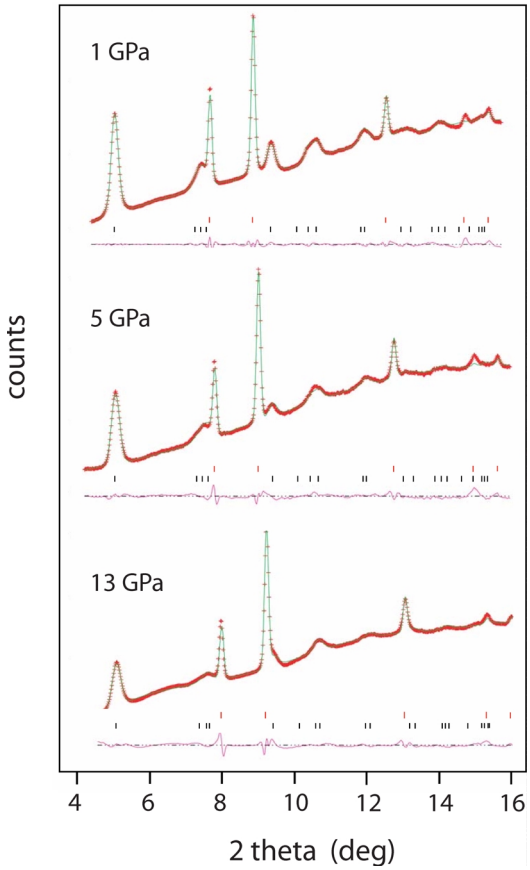

Fig. 2. Results of full profile refinements of XRD patterns at various pressures (λ = 0.31 Å; upper tickmarks = LiF; lower tickmarks = anatase $Zr_{0.1}Ti_{0.9}O_2$).

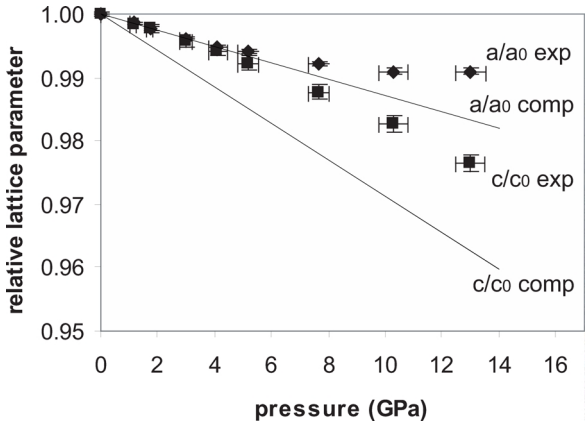

Fig. 3a. Relative lattice parameters a/a_0 and c/c_0 as a function of pressure; exp = experimental XRD data for $Zr_{0.1}Ti_{0.9}O_2$ nano anatase; comp = results of *ab initio* computations for bulk $Zr_1Ti_7O_{16}$ anatase.

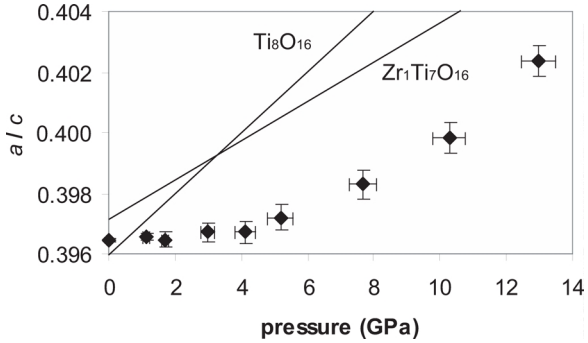

Fig. 3b. Ratio of the lattice parameters a/c of Zr-doped nano anatase (experiments, diamonds) as well as anatase Ti_8O_{16} and $Zr_1Ti_7O_{16}$ (computed, lines).

The XRD data of the sample at ambient conditions were used to estimate the crystallite size of the starting material. We used the TOPAS-ACADEMIC software [40] for convolution-based profile fitting [41] and refined the microstructure. The diffraction spectrum of a CeO standard was used to determine the source emission profile and instrumental contribution to peak broadening. The effects of crystallite size and strain on the peak broadening were analyzed using the double-Voigt approach [42]. Integral-breadth-based volume-weighted mean column height L_{Vol_IB} of coherently diffracting domains as well as mean strain values e_0 [41] were obtained simultaneously, resulting in L_{Vol_IB} = 11.0(3) nm and e_0 = 22(1)%, while the residuals of the fit are *R*wp = 1.370. The considerable amount of strain is related to the high contribution of the distorted surface for nanocrystalline material. The estimate of crystallite size from L_{Vol_IB} depends on the

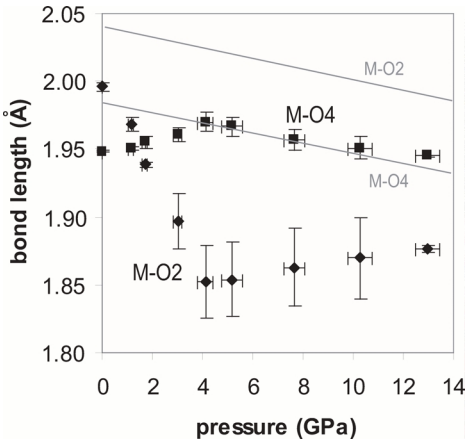

Fig. 4. Metal-oxygen bond lengths of the MO_6 octahedra. M–O2 = average bond length of (Ti, Zr) and apical oxygen atom O2; M–O4 = average bond length of (Ti, Zr) and equatorial oxygen atom O4; black points = experimental results from XRD; grey continued lines = results from *ab initio* computations.

particular crystallite shape and on the size distribution of the crystallites. For monodispers spherical crystallites with diameter D, the following equation is applicable: $D = 4/3\ L_{Vol\_IB}$ [43, 44]. The resulting value for the starting material is D = 14.7(4) nm, which is in excellent agreement with the estimate from TEM analysis of 15(5) nm.

The Zr-doped nanoanatase was observed as a pure phase up to a pressure of 13 GPa, as indicated by the refined X-ray diffraction patterns (Fig. 2). The trends of the variations of the lattice parameters are presented in Fig. 3. The slope of the relative lattice parameter a/a_0 decreases for pressures > 4 GPa, indicating a decrease in compressibility of the a parameter at higher pressures (Fig. 3a). Because the slope c/c_0 remains the same, the ratio of a/c strongly increases at $p > 4$ GPa (Fig. 3b). A difference in the slope is also observed for a number of other parameters, *e. g.* the average M–O bond lengths in the octahedra (Fig. 4) or the oxygen positions (Table 2) indicating a change in the compression behavior at a pressure of ~ 4 GPa. The variation of the M–O4 bond length is only slightly larger than the error of data points and therefore can be taken as almost constant. The M–O2 bond length in contrast has a negative slope at pressures < 4 GPa and a positive slope at higher pressures. The oxygen positions follow a similar trend: the z coordinate decreases in the former p range and increases in the latter. It is worth noting that the change in compression behavior is not related to a phase transformation, as can be seen from the re-

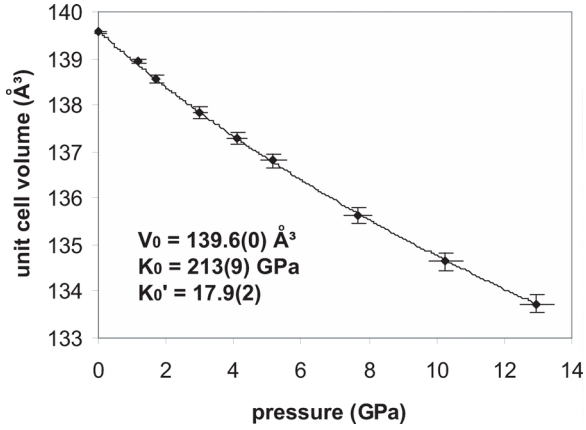

Fig. 5. Experimental room temperature pressure-volume data of nano crystalline $Zr_{0.1}Ti_{0.9}O_2$ anatase (diamonds) and a Birch-Murnaghan equation of state fit (curve).

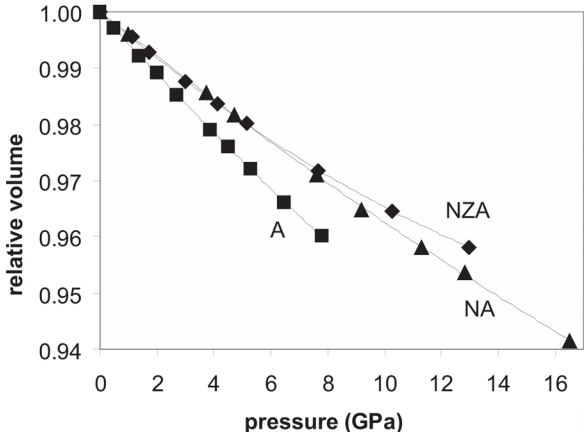

Fig. 6. Various Birch-Murnaghan equation of state fits of experimental pressure-volume data on (A) anatase [20], (NA) nano anatase [21] and (NZA) nano crystalline Zr-doped anatase (this study).

fined X-ray pattern (Fig. 2), which clearly indicates the presence of only anatase and LiF up to a pressure of 13 GPa.

The pressure *versus* volume data obtained from full profile analysis were fitted to a third order Birch-Murnaghan equation of state, resulting in V_0 = 139.6(0) Å^3, K_0 = 213(9) GPa and K' = 17.9(2) (Fig. 5). Since for most materials K' has a value of ~ 4, the value of 17.9(2) appears to be extremely high. However, a decrease of the slope of cell volume *versus* pressure is consistent with the change in compression behavior at ~ 4 GPa. To make our data comparable to other studies, where K' = 4, we fitted our data to a second order EoS, resulting in a much higher K_0 of

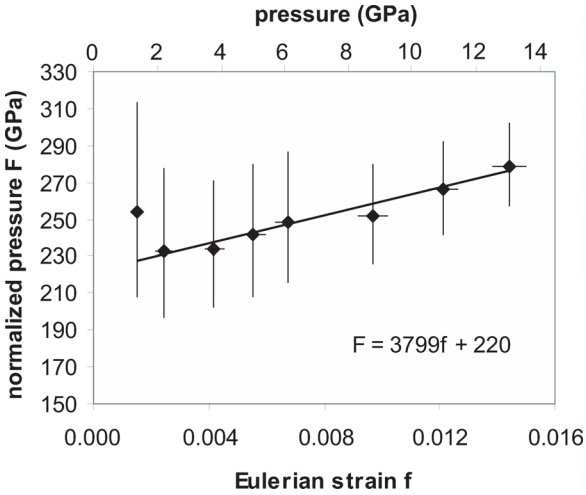

Fig. 7. *F-f* plot of experimental data on $Zr_{0.1}Ti_{0.9}O_2$ nano anatase based on the Birch-Murnaghan equation of state. The data are described by a third-order truncation of the equation of state and the linear fit has a slope of 3 K_0 ($K' - 4$)/2.

278(7) GPa. Due to the change in compression behavior at ~ 4 GPa, we also fitted the second order EoS for different pressure ranges, again keeping $K' = 4$. The results for 0 – 5 GPa are K_0 = 249(6) GPa, and for 4 – 13 GPa K_0 = 301(1) GPa showing that the bulk modulus strongly increases with pressure.

Fig. 6 shows a comparison of Birch-Murnaghan EoS fits for experiments on TiO_2 anatase [20] and TiO_2 nanoanatase [21]. Anatase has the highest compressibility. In the pressure range of 0 – 6 GPa, the Zr-doped nanoanatase of this study has the same compressibility as TiO_2 nanoanatase. Due to the increasing bulk modulus at higher pressures the compressibility of the Zr-doped material is smaller than that of the pure nanoanatase at $p > 6$ GPa.

Fig. 7 shows a plot of Birch's normalized pressure F *versus* the Eulerian strain f with: $F = \mathrm{P}/(3f(2f+1))^{5/2}$ and $f = 0.5(V_0/V^{2/3} - 1)$. The data were fitted to $F = 3799f + 221$, resulting in K_0 = 221 GPa. Given that the slope of the fit is $3K_0(K' - 4)/2$, it follows that K' = 15.5. These results are compatible with the results from the Birch-Murnaghan fit presented above.

Computational results

From the computed internal energies for different cell volumes of TiO_2 and Zr-doped anatase (Ti : Zr = 7 : 1) we obtain the EoS parameters by fitting the *E-V* relation. In agreement with experiment we find that the doping of TiO_2 anatase with Zr expands the zero pres-

Table 3. Internal energy and configuration of different supercells.

Ti:Zr	cell	Zr–Zr (Å)	E (eV)	k
1:7	$a \times b \times 2c$	3.785 (a,b)	−215.73	$12 \times 12 \times 2$
1:7	$2a \times b \times c$	3.789 (a)	−215.64	$6 \times 12 \times 4$
2:14	$2a \times 2b \times c$	5.377	−215.58	$4 \times 4 \times 4$
0:8	$2a \times b \times c$	–	−215.28	$6 \times 12 \times 4$

sure volume by $\sim 3\%$ and decreases the compressibility markedly. We obtain $K' = 4.0$ for both TiO_2 and $(Ti_7Zr)O_{16}$ which differs from the experimental results for Zr-doped nanocrystalline anatase (Table 1). In addition to the EoS we use the computational results to compare the relative lattice parameters (Fig. 3) and bond lengths (Fig. 4). The calculated slopes of relative lattice parameters a/a_0 and c/c_0 are constant and have a more negative slope than the experimental data (Fig. 3). The bond lengths of the metal to the equatorial oxygen atoms of a polyhedron (M–O4) are smaller than the ones to the apical atoms (M–O2), in contrast to experimental data where the polyhedra are found largely incompressible. The failure to reproduce the experimental data for the distortion of the polyhedra is in part responsible for the prediction of more compressible polyhedra (Table 1).

The consideration of alternative supercells at a volume of 11 Å^3 per atom is shown in Table 3 and indicates that the Zr atoms in anatase have a tendency to cluster. The cell with evenly spread Zr atoms $(2a \times 2b \times c)$ with the longest possible Zr–Zr distance for nearest neighbors of 5.377 Å is energetically least favorable (Table 3). The cell $a \times b \times 2c$ in which the nearest neighbors with a Zr–Zr distance of 3.785 Å are found in the directions parallel to the *a* and *b* axis has the lowest energy.

Discussion and Conclusions

The experimental results on Zr-doped nanoanatase show a significant change in compression behavior at pressures > 4 GPa: The slope of *a*/*c* strongly increases, the slope of the bond length M–O2 of the octahedra changes from negative to positive and the *z* coordinate of the oxygen atom in the Wyckoff position *8e*, the only free atomic coordinate, changes its trend. This change in compression behavior can be understood by considering the crystal structure. Fig. 8 shows the structure of anatase in the *bc* plane. Each Ti is surrounded by an octahedron of six oxygen atoms. The octahedra are linked *via* edges and build a zig-zag chain parallel to *a* as well as *b*. The chains are stacked antiparallel to the *c* axis

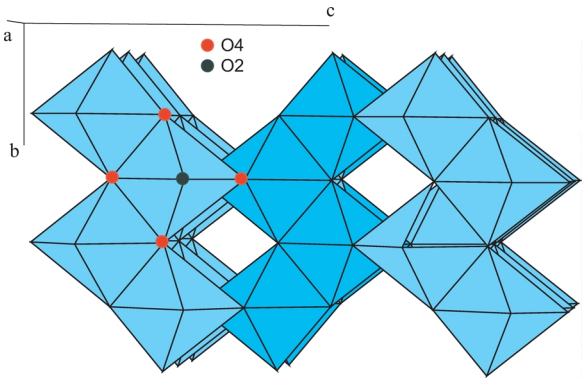

Fig. 8. Structure of anatase; the lattice is shown in the *bc* plane, dimensions are $3a \times 2b \times 2c$. O4 = equatorial oxygen atoms (edge sharing); O2 = apical oxygen atoms (corner sharing).

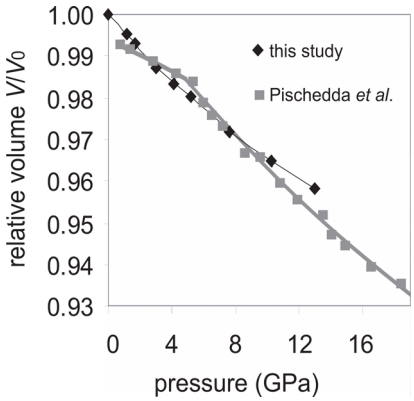

Fig. 9. Volume-pressure data of $Zr_{0.1}Ti_{0.9}O_2$ nano anatase (this study) and nano crystalline anatase TiO_2 [46]. The slope of the curve decreases at ~ 5 GPa for Zr-doped nano anatase and increases for TiO_2 nano anatase.

and, as our data suggest, can be compressed $\| c$ with the same rate over the whole pressure range analyzed. However, along the directions *a* and *b*, the chains can be compressed more readily at pressures < 4 GPa than at higher pressures. This phenomenon also affects the bond lengths and thus the distortion of the octahedra: At pressures below 4 GPa the degree of distortion of individual octahedra increases, while above 4 GPa the distortion decreases.

The results of the computations do not show a significant change in the slope for the relative lattice parameters (Fig. 3), neither for the bond lengths within the octahedra (Fig. 4) nor the *z* positions of the oxygen atoms (Table 2) as a function of pressure. The change in compression behavior at ~ 4 GPa as found in the experiments is not reproduced by the first principle cal-

culations. This is not surprising because the periodic boundary conditions of the computations calculate an infinite crystal and are not constrained for the compression of a nanocrystalline material, in which deviatoric stresses play an important role. Bulk or polycrystalline Zr-doped anatase could not be prepared because the annealing process would lead to a recrystallization of the material into rutile above ~ 700 °C (*e. g.* [45]). Even though we used the pressure medium LiF, which is characterized by a small shear modulus [30], the spatial pressure distribution within our cell is most likely not even and deviatoric stresses might play an important role.

The experimental studies by Swamy [21] and Pischedda *et al*. [46] show a higher bulk modulus for nanocrystalline TiO_2 anatase than for bulk anatase (Fig. 9). The authors fitted the pressure-volume data to a second order Birch-Murnaghan EoS ($K' = 4$, fixed) and obtained a value for the bulk modulus of 243 GPa in the pressure range of 0 – 20 GPa [21] and a value of 237 GPa in the range of 6 – 18 GPa [46]. The values are well comparable to the fitted EoS from data on Zr-doped anatase: In the pressure range of 0 – 4 GPa we fitted a K_0 of 249 GPa (compare Table 1). We therefore conclude that the bulk modulus of nanocrystalline anatase is systematically higher by about 30 – 35% than of the bulk material.

However, none of the previous studies on anatase showed a decrease in compressibility similar to the experimental results on Zr-doped nanoanatase. The tendency of Zr-atoms to form clusters as shown by our *ab initio* computations can lead to a variation of structural parameters, supporting a change in compression behavior. The clustering may even be supported by deviatoric stresses in the sample chamber which can be expected during the compression of nanocrystals.

Another important fact which should be taken into account is the phase transition from TiO_2 anatase to the high-pressure phase TiO_2-II which was observed at pressures between 2.5 and 7 GPa in all single crystal [11, 23] and several powder XRD studies [24 – 26]. This phase transition was suppressed in our experiments as well as in other work on nanocrystalline material [21, 23, 27]; however, in the same pressure region, a change in compression behavior is found for Zr-doped nano anatase (this study) as well as for pure nano anatase [46].

We conclude that the strong decrease of compressibility at higher pressures is related to the nanocrystallinity of the anatase material. It appears that Zr-doping and the tendency of clustering of Zr-atoms can affect the structural parameters and influence the elastic properties: opposed to the conclusion one would draw from comparison of elastic constants for TiO_2 and ZrO_2 polymorphs (see Table 1), the incorporation of Zr into TiO_2 anatase results in an increasing bulk modulus. Further studies to analyze if this phenomenon can also be observed for other polymorphs are an interesting task.

Acknowledgements

We thank the Elitenetzwerk Bayern for funding of the project and Tiziana Boffa-Ballaran for reviewing the manuscript. Portions of this work were performed at GeoSoilEnviroCARS (Sector 13), Advanced Photon Source (APS), Argonne National Laboratory. GeoSoilEnviroCARS is supported by the National Science Foundation – Earth Sciences (EAR-0217473), Department of Energy – Geosciences (DE-FG02-94ER14466) and the State of Illinois. Use of the APS was supported by the U.S. Department of Energy, Office of Science, Office of Basic Energy Sciences, under Contract No. W-31-109-ENG-38.

[1] M. Dondi, F. Matteucci, G. Cruciani, J. Solid State Chem. **179**, 233 (2006).
[2] C. E. F. Costa, S. C. L. Crispim, S. J. G. Lima, C. A. Paskocimas, E. Longo, J. Thermal Analysis and Calorimetry **75**, 467 (2004).
[3] F. J. Parker, J. Amer. Cer. Soc. **73**, 929 (1990).
[4] L. Cerchez, S. Constantinescu, British Ceramic Transactions **99**, 260 (2000).
[5] B. M. Reddy, A. Khan, Catalysis Reviews-Science and Engineering **47**, 257 (2005).
[6] V. Swamy, J. D. Gale, L. S. Dubrovinsky, J. Phys. Chem. Sol. **62**, 887 (2001).
[7] A. El Goresy, M. Chen, P. Gillet, L. Dubrovinsky, G. Graup, R. Ahuja, Earth and Planetary Science Letters **192**, 485 (2001).
[8] J. S. Olsen, L. Gerward, J. Z. Jiang, J. Phys. Chem. Sol. **60**, 229 (1999).
[9] A. C. Withers, E. J. Essene, Y. X. Zhang, Contributions to Mineralogy and Petrology **145**, 199 (2003).
[10] V. Swamy, N. A. Dubrovinskaia, L. S. Dubrovinsky, J. Alloys Comp. **340**, 46 (2002).
[11] K. Lagarec, S. Desgreniers, Solid State Commun. **94**, 519 (1995).
[12] N. A. Dubrovinskaia, L. Dubrovinsky, R. Ahuja, V. B. Prokopenka, V. Dmitriev, Phys. Rev. Let. **87**, 275501 (2001).

[13] N. A. Dubrovinskaia, L. S. Dubrovinsky, V. Swamy, R. Ahuja, High Pres. Res. **22**, 391 (2002).
[14] L. S. Dubrovinsky, N. A. Dubrovinskaia, V. Swamy, J. Muscat, N. M. Harrison, R. Ahuja, B. Holm, B. Johansson, Nature **410**, 653 (2001).
[15] M. Mattesini, J. S. de Almeida, L. Dubrovinsky, N. Dubrovinskaia, B. Johansson, R. Ahuja, Phys. Rev. B **70**, 212101 (2004).
[16] R. E. Latta, E. C. Dudersta, R. E. Fryxell, J. Nuc. Mat. **35**, 345 (1970).
[17] J. M. Leger, P. E. Tomaszewski, A. Atouf, A. S. Pereira, Phys. Rev. B **47**, 14075 (1993).
[18] O. Ohtaka, H. Fukui, T. Kunisada, T. Fujisawa, K. Funakoski, W. Utsumi, T. Irifune, K. Kuroda, T. Kikegawa, Phys. Rev. B **6317**, 174108 (2001).
[19] B. Jiang, J. M. Zuo, N. Jiang, M. O'Keeffe, J. C. H. Spence, Acta Crystallogr. Section A **59**, 341 (2003).
[20] V. Swamy, L. S. Dubrovinsky, J. of Phys. Chem. Sol. **62**, 673 (2001).
[21] V. Swamy, L. Dubrovinsky, N. A. Dubrovinskaia, A. S. Simionovici, M. Drakopoulos, V. Dmitriev, H. P. Weber, Solid State Commun. **125**, 111 (2003).
[22] F. Birch, Phys. Rev. **71**, 809 (1947).
[23] T. Arlt, M. Bermejo, M. A. Blanco, L. Gerward, J. Z. Jiang, J. S. Olsen, J. M. Recio, Phys. Rev. B **61**, 14414 (2000).
[24] T. Ohsaka, S. Yamaoka, O. Shimomura, Solid State Commun. **30**, 345 (1979).
[25] J. Haines, J. M. Leger, Physica B **192**, 233 (1993).
[26] G. R. Hearne, J. Zhao, A. M. Dawe, Y. Pischedda, M. Maaza, M. K. Nieuwoudt, P. Kibasomba, O. Nemraoui, J. D. Comins, M. J. Witcomb, Phys. Rev. B **70**, 134102 (2004).
[27] Z. W. Wang, S. K. Saxena, V. Pischedda, H. P. Liermann, C. S. Zha, J. Phys.-Condens. Matter **13**, 8317 (2001).
[28] N. Dubrovinskaia, L. Dubrovinsky, Rev. Sci. Instru. **74**, 3433 (2003).
[29] E. Holbig, M. Bockmeyer, L. Dubrovinsky, P. Loebmann, J. Alloys Comp. (submitted).
[30] T. Yagi, J. Phys. Chem. Solids **39**, 563 (1977).
[31] A. Hammersley, Computer program FIT2D, ESRF, Grenoble, 1998.
[32] A. C. Larson, R. B. Von Dreele, Los Alamos National Laboratory Report LAUR, 86 (2000).
[33] B. H. Toby, J. Appl. Cryst. **34**, 210 (2001).
[34] J. Hafner, Acta Materialia **48**, 71 (2000).
[35] J. P. Perdew, J. A. Chevary, S. H. Vosko, K. A. Jackson, M. R. Pederson, Phys. Rev. B **46**, 6671 (1992).
[36] G. Kresse, J. Hafner, Phys. Rev. B **47**, 558 (1993).
[37] G. Kresse, J. Furthmüller, Phys. Rev. B **54**, 11169 (1996).
[38] M. Horn, C. F. Schwerdt, E. P. Meagher, Z. Kristallogr. **136**, 273 (1972).
[39] H. J. Monkhorst, J. D. Pack, Phys. Rev. B **13**, 5188 (1976).
[40] A. Coelho, TOPAS-Academic Users Manual, http://pws.prserv.Net/Alan.Coelho/ (2005).
[41] A. Kern, A. Coelho, R. W. Cheary, in E. J. Mittemeijer, P. Scardi (eds): Diffraction Analysis of the Microstructure of Materials, p. 17, Springer, Berlin (2004).
[42] D. Balzar, H. Ledbetter, J. Appl. Crystallogr. **26**, 97 (1993).
[43] D. Balzar, J. Appl. Cryst. **25**, 559 (1992).
[44] N. C. Popaa, D. Balzar, J. Appl. Cryst. **35**, 338 (2002).
[45] S. A. Borkar, S. R. Dharwadkar, J. Thermal Analysis and Calorimetry **78**, 761 (2004).
[46] V. Pischedda, G. R. Hearne, A. M. Dawe, J. E. Lowther, Phys. Rev. Let. **96**, 035509 (2006).
[47] L. Gerward, J. S. Olsen, J. Appl. Crystallogr. **30**, 259 (1997).
[48] W. Luo, S. F. Yang, Z. C. Wang, Y. Wang, R. Ahuja, Solid State Commun. **133**, 49 (2005).
[49] S. Desgreniers, K. Lagarec, Phys. Rev. B **59**, 8467 (1999).
[50] S. K. Chan, J. Amer. Ceram. Soc. **74**, 1742 (1991).
[51] R. E. Cohen, M. J. Mehl, L. L. Boyer, Physica B & C **150**, 1 (1988).
[52] J. K. Dewhurst, J. E. Lowther, Phys. Rev. B **57**, 741 (1998).
[53] P. Bouvier, E. Djurado, G. Lucazeau, T. Le Bihan, Phys. Rev. B **62**, 8731 (2000).
[54] O. Ohtaka, D. Andrault, P. Bouvier, E. Schultz, M. Mezouar, J. Appl. Crystallogr. **38**, 727 (2005).
[55] J. Haines, J. M. Leger, A. Atouf, J. Amer. Ceram. Soc. **78**, 445 (1995).